doi:10.1038/nature09450

Supplementary Table 1 Summary of kinetic parameters

DPTAP (%)	d_s (nm)	V_{max} (nm s^{-1})	K_m (μM)	k_1 (μM^{-1} s^{-1})	k_2 (s^{-1})
0	37.2 ± 12.5	403 ± 7	5.4 ± 0.5	2.0 ± 0.9	10.8 ± 3.8
1	37.7 ± 8.8	384 ± 8	7.1 ± 0.6	1.4 ± 0.5	10.2 ± 2.6
5	41.1 ± 7.5	295 ± 9	7.7 ± 1.0	0.9 ± 0.3	7.2 ± 1.5
Forkey *et al.* (2003)[3]		453 ± 10	11.7 ± 1.2	1.1 ± 0.2	12.0 ± 1.7
Baker *et al.* (2004)[4]		380 ± 40	6.1 ± 1.1	~1.7*	~10.6*

*The values were calculated by assuming the step size to be ~36 nm.

Supplementary Table 1 | Summary of kinetic parameters. Kinetic parameters were obtained using the relationships $V = V_{max} / (1 + K_m / [ATP])$ and $V = d_s / (1/k_1[ATP] + 1/k_2)$, where V is the average translocation velocity in a given [ATP] (Supplementary Fig. 2), V_{max} is the maximum translocation velocity, K_m is the apparent Michaelis-Menten constant, d_s is the average step size, and k_1 and k_2 are the second-order ATP binding rate constant and first-order ADP dissociation rate constant, respectively. The second relationship holds because ADP release is a major rate-limiting step, ATP binding is also a rate-limiting step in low [ATP], other chemical steps occur much faster[1], and one discrete translocation is tightly coupled to one ATP hydrolysis[2]. All values represent best-fit results ± s.d. When DPTAP-free lipid bilayers were used, V_{max} was 403 ± 7 nm s^{-1}, which is similar to that obtained using fluorescence microscopy under the same buffer condition[3,4], indicating that tip-sample and surface-sample interactions have negligible effects on motor activity. However, in the absence of surface-sample attraction, M5-HMM occasionally did not travel sideways along actin filaments; hence, it was difficult to acquire high-resolution images since AFM is inefficient for visualising molecules not supported on a surface. Therefore, the addition of the positively charged lipid was necessary to improve image quality and experimental efficiency, despite a modest decrease in average translocation velocity.

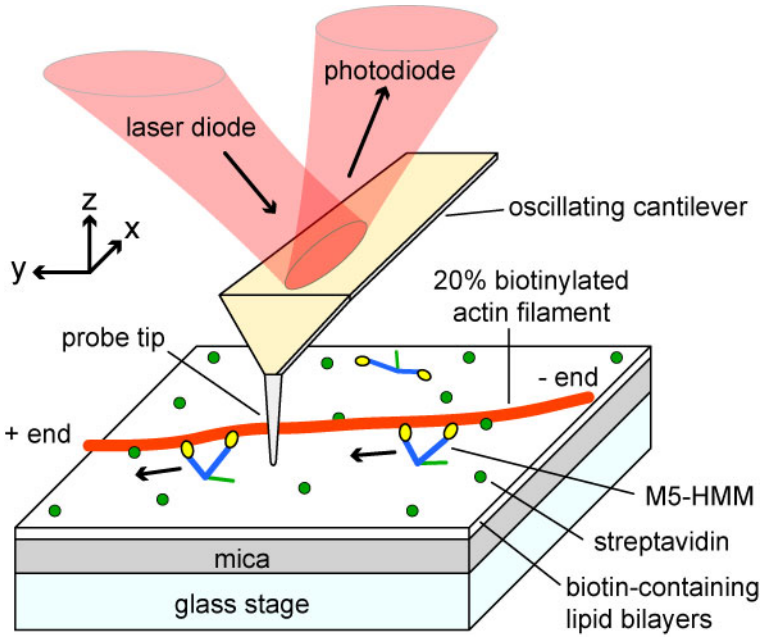

Supplementary Figure 1 | Schematic of assay system for HS-AFM imaging (not scaled). A mica surface was fully covered with biotin-containing lipid bilayers. Streptavidin molecules (green circles) were partially deposited on the substrate. Biotinylated actin filaments were immobilised on the bilayer surface through streptavidin molecules. M5-HMM was deposited on the lipid bilayers. All imaging experiments were performed in the tapping mode using a laboratory-built high-speed AFM apparatus[5,6].

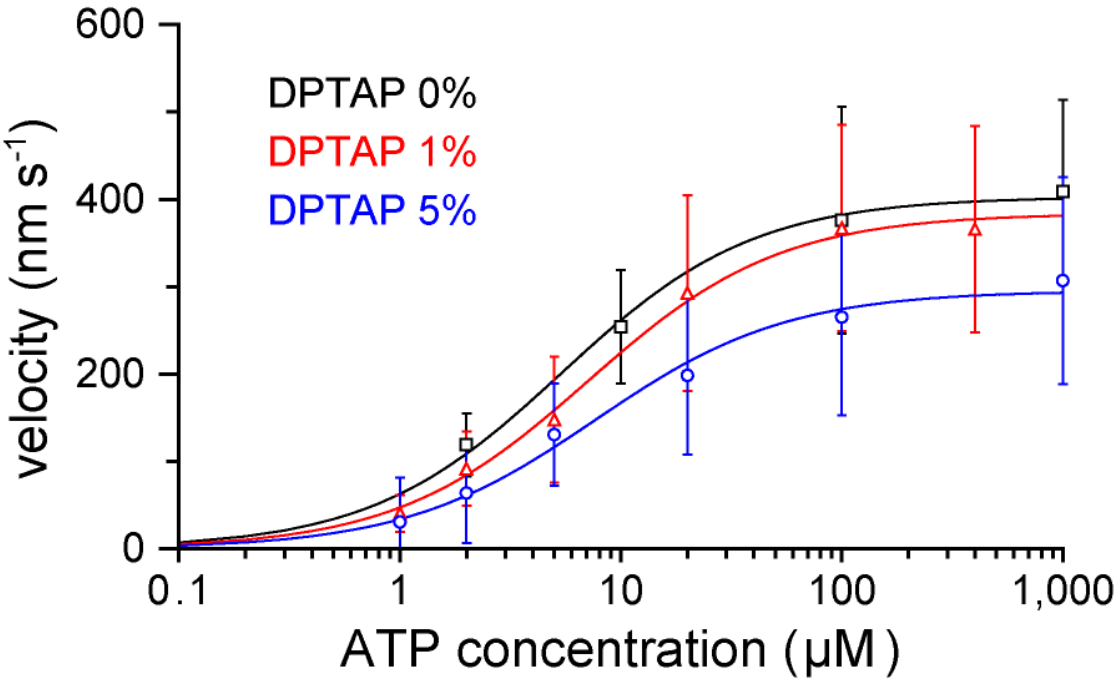

Supplementary Figure 2 | Translocation velocity of M5-HMM observed by HS-AFM. The observations were performed in various [ATP] using planar lipid bilayer surfaces containing different fractions of positively charged lipid DPTAP. Walking M5-HMM molecules were imaged at 146.3 ms frame^{-1} (400 × 125 nm^2 scan range, 80 × 25 pixels). In ATP higher than 20 μM, very shortly dwelled states were missed. In this case, translocation velocity was obtained from movies in which at least four instances of dwelling at different locations along an actin filament were captured on video. The translocation velocity in a given [ATP] was thus measured and its average (V) was fitted to the relationship $V = d_s / (1/k_1[ATP] + 1/k_2)$ (see Supplementary Table 1). The curves are best-fit results. Each data point was obtained from the translocation trajectories of more than 100 molecules (103-276). Error bars, ± s.d. The fitting results are summarised in Supplementary Table 1.

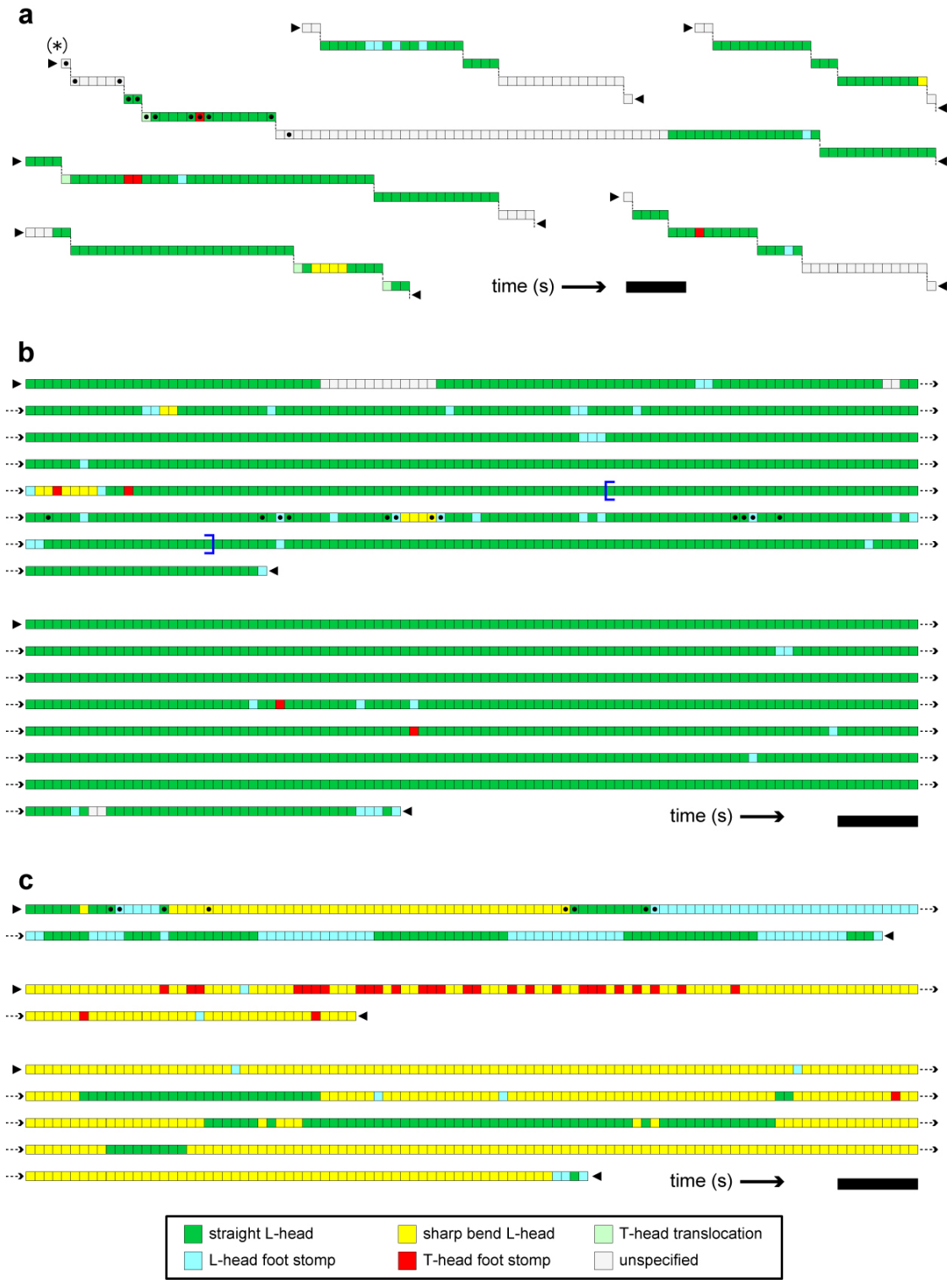

Supplementary Figure 3 | Time courses showing the molecular conformations under different nucleotide conditions. (a) Six typical time courses in 1 μM ATP. Each time course starts from the right-pointing triangle and ends with the left-pointing

triangle. Discrete ~36 nm steps occur at the vertical dashed lines. Each box corresponds to a video frame. The colour code of the boxes is given at the bottom of the figure. The same colour code is also used for (b) and (c). Each box with a black dot, which is contained in the asterisk-labelled time course, corresponds to an AFM image shown in Fig. 1a (Supplementary Movie 1a). Scale bar, 1 s. (b) Two typical time courses in 50 μM ADP. Each box with a black dot in the first time course corresponds to an AFM image in Fig. 2a (Supplementary Movie 3). Scale bar, 3 s. (c) Three typical time courses in the NF condition. Each box with a black dot in the first time course corresponds to an AFM image in Fig. 2c (Supplementary Movie 5a). The molecule observed in the second time course is shown in Supplementary Movie 5b. Scale bar, 3 s.

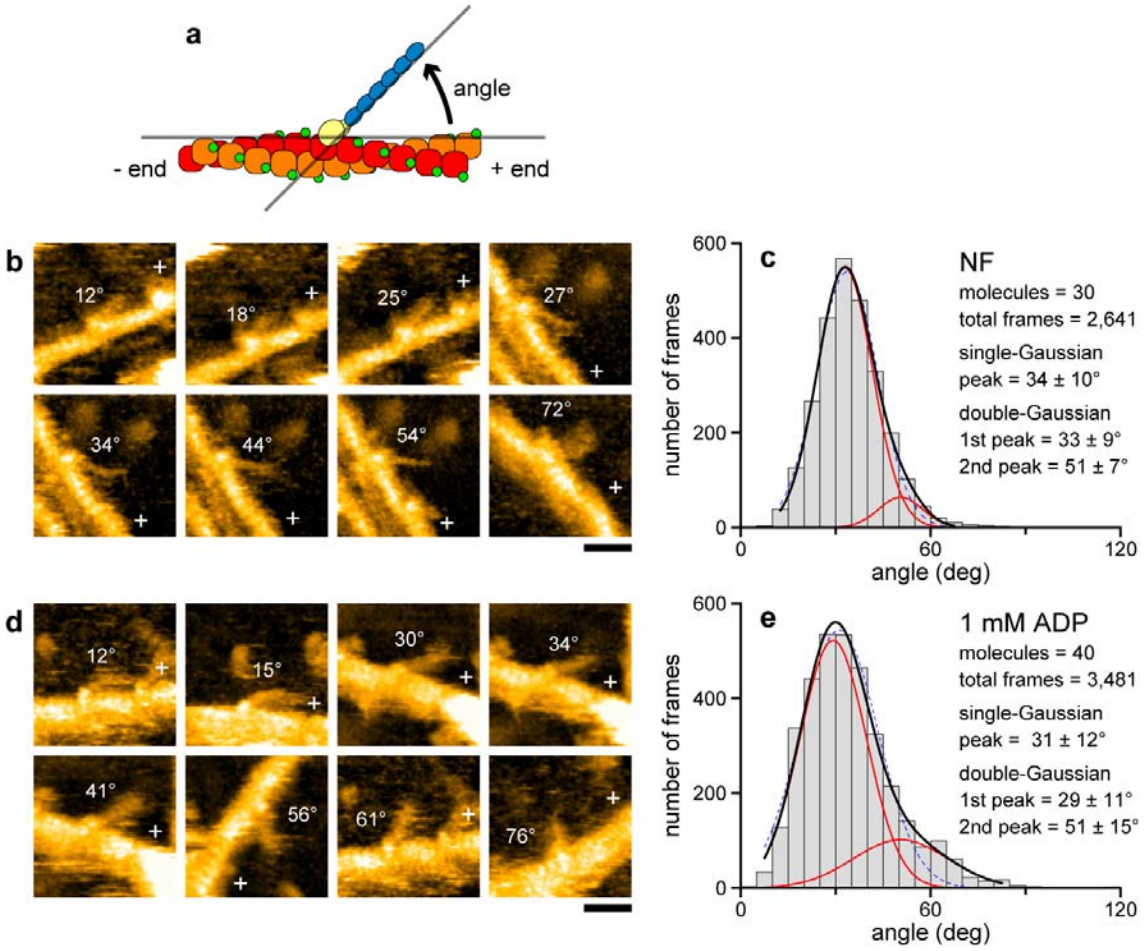

Supplementary Figure 4 | Angle distributions of single-headed M5 bound to actin. The single-headed M5 is formed by natural unwinding of the short tail of two-head bound M5-HMM. (a) Schematic showing the angle measured. (b), (d) AFM images of single-headed bound M5 in the NF and 1 mM ADP conditions, respectively. The plus ends of actin filaments are indicated with '+'. The measured angles are shown in the images. Imaging rate, 333.2 ms frame^{-1}. Scale bar, 30 nm. (c), (e) Histograms of the angle measured for single-headed bound M5 in the NF and 1 mM ADP conditions, respectively. Blue broken lines, single-Gaussian fit results; black solid lines, double-Gaussian fit results; red lines, Gaussian components in double-Gaussian fit. All fits were restricted to bins with > 10 counts. All values for peak angles represent mean ± s.d. The two-Gaussian distributions are statistically significant judging from the *F*-test results: $p < 0.05$ for the NF condition; $p < 10^{-6}$ for the 1 mM ADP condition.

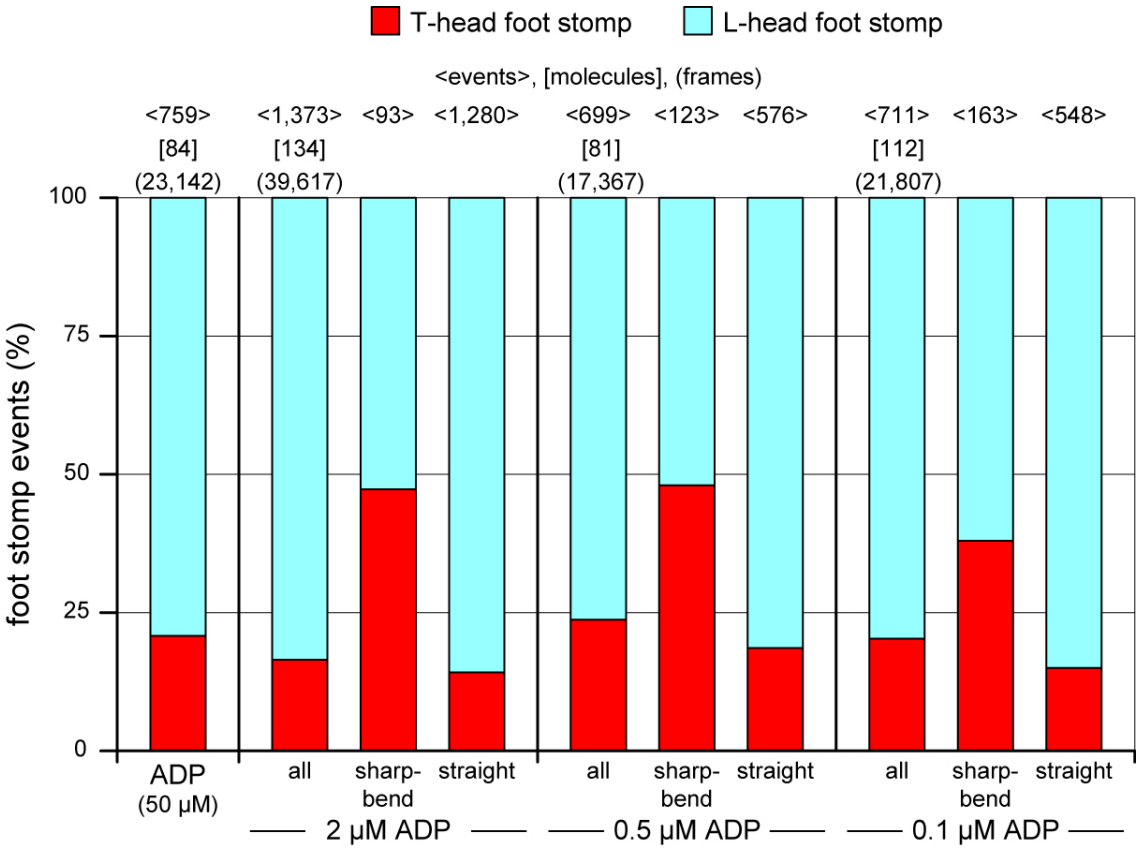

Supplementary Figure 5 | Proportion of foot stomp events that occur at L- and T-heads in various [ADP]. The proportion depends on the L-head conformation (straight or sharp bend); the proportion difference between the L- and T-heads becomes smaller when the L-head assumes the sharp bend conformation, irrespective of [ADP]. In 50 μM ADP, the L-head almost always assumes the straight conformation. Foot stomp events counted without distinguishing between the two conformations of the L-head are indicated by 'all'. The numbers in <events>, [molecules], and (frames) represent the respective numbers examined for foot stomp events observed under the respective conditions.

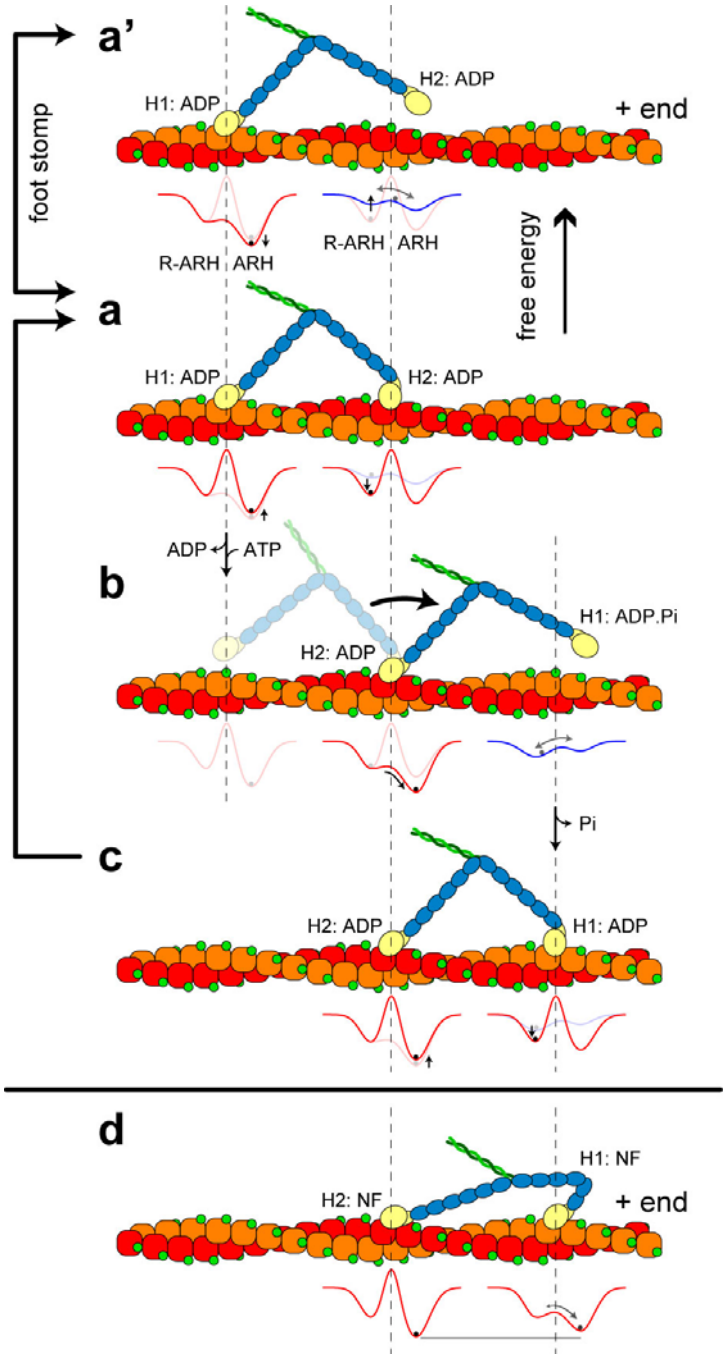

Supplementary Figure 6 | Walking mechanism of myosin V highlighting the energy landscapes of actin-bound L- and T-heads. The red lines represent the energy landscapes of actin-bound heads in the respective states. The blue lines represent the energy landscapes of detached heads. The left and right sides partitioned by the vertical dashed lines of each energy landscape shown in red correspond to the reverse arrowhead (R-ARH) and arrowhead (ARH) conformations, respectively. The left and

right sides partitioned by the vertical lines of each energy landscape shown in blue correspond to the pre-stroke and post-stroke conformations, respectively. The black dot in each energy landscape indicates the most probable position of the corresponding head in the energy landscape. Each energy landscape shown in a faint colour represents that in the previous state. (a) Initial state of the step cycle in which both heads (H1 and H2) carry bound ADP. In this chemical state, foot stomping more frequently occurs at the L-head than at the T-head, and therefore, the free energy level of the L-head is higher than that of the T-head. The L-head-bound ADP is very stable. (a') State in which the L-head detaches from actin while foot stomping. The detached L-head is in equilibrium between the pre-stroke and post-stroke conformations. The T-head is in the lowest-energy state as the intramolecular strain is released. Even in this state, the T-head can swing backward with a low probability. Transitions between (a) and (a') occur alternately. (b) ADP release, subsequent ATP binding, and resulting detachment at the T-head. The T-head detachment removes the high potential barrier in the energy landscape of the L-head, thus, the L-head spontaneously descends to the bottom of the energy landscape, swinging from the R-ARH orientation to the ARH orientation. The T-head rotationally diffuses around the advancing neck-neck junction to search for an actin subunit to attach to. The ADP-Pi-bound L-head possibly preferentially assumes the pre-stroke conformation as reported previously[7,8]. (c) The detached head is reattached and then phosphate is immediately released to return to the original two-head bound state (a), resulting in a ~36 nm advance. As the sharp bend conformation is rarely observed on the leading neck even in low [ATP] (0.1 μM and 1 μM), M5 only moves forward by repeating the changes described in (a), (b), and (c) in this order. (d) The sharp bend conformation is frequently observed in the leading neck in the NF condition. In this structural state, the two heads are bound to actin in the ARH orientation (at least around the motor domains) with similar affinities, and thus, the foot stomp occurs on the two heads at nearly equal frequencies.

Legends for Supplementary Movies

Supplementary Movie 1 | High-speed AFM movies showing unidirectional processive movement of M5-HMM. The dynamic process in 1 μM ATP was filmed at 146.7 ms frame^{-1} (6.8 frames s^{-1}) and the movie is played at 7 frames s^{-1}. To track the M5-HMM molecules, the scan area was moved (a, c, d). Foot stomp events are marked with light-blue (L-head) and red triangles (T-head). (a) Scan range, 130 × 65 nm^2 with 80 × 40 pixels. Twelve frames are selected and shown in Fig. 1a. The time course of the molecular conformations is shown in the asterisk-labelled sequential boxes (Supplementary Fig. 3a). (b) Scan area, 125 × 62.5 nm^2 with 80 × 40 pixels. (c), (d) Typical movies showing long processive runs. (c) Scan range, 130 × 65 nm^2 with 80 × 40 pixels; the whole imaging area, 560 × 160 nm^2; number of steps observed, 15. (d) Scan range, 150 × 75 nm^2 with 80 × 40 pixels; whole imaging area, 500 × 120 nm^2; number of steps observed, 14.

Supplementary Movie 2 | High-speed AFM movies showing hand-over-hand movement of M5-HMM. The dynamic process was filmed at 146.7 ms frame^{-1} (6.8 frames s^{-1}) and the obtained movies are played at 7 frames s^{-1}. Additional streptavidin molecules were scattered on the biotin-containing surface to slow the step movement. Foot stomp events observed at the L-head are marked with light-blue triangles (a, e). No foot stomping at the T-head is observed in these five movie clips. (a), (b) In 1 μM ATP. Scan area, 150 × 75 nm^2 with 80 × 40 pixels. (c) In 2 μM ATP. Scan area, 130 × 65 nm^2 with 80 × 40 pixels. Frames selected from (a) and (c) are shown in Figs. 1d and 1e, respectively. (d), (e) In 1 μM ATP. Scan area, 110 × 75 nm^2 with 80 × 50 pixels.

Supplementary Movie 3 | High-speed AFM movie of two-head bound M5-HMM observed in 50 μM ADP. The sample was filmed at 333.2 ms frame^{-1} (3 frames s^{-1}) and the movie clip is played at 3 frames s^{-1}, from which 12 frames are selected and shown in Fig. 2a. The conformational states observed in the movie clip are shown in the first time course of Supplementary Fig. 3b (between the square brackets). Scan area, 90 × 90 nm^2 with 80 × 80 pixels. Foot stomp events observed at the L-head are marked with light-blue triangles. No foot stomping at the T-head is observed in this movie clip.

Supplementary Movie 4 | High-speed AFM movies showing unwinding of short coiled-coil tail of M5-HMM. (a), (b) Two different samples in 50 μM ADP were filmed

at 333.2 ms frame^{-1} (3 frames s^{-1}) and the obtained movies are played at 3 frames s^{-1}. AFM images selected from (b) are shown in Fig. 2b. Rewinding was not observed. Scan area, 90 × 90 nm^2 with 80 × 80 pixels. (c), (d) Two different samples in ADP were filmed at 333.2 ms frame^{-1} (3 frames s^{-1}) and the obtained movies are played at 3 frames s^{-1}. Unwinding and rewinding of the tail were observed. Scan area, 90 × 90 nm^2 with 80 × 80 pixels. (c) In 50μM ADP, (d) in 1 mM ADP.

Supplementary Movie 5 | High-speed AFM movies of two-head bound M5-HMM observed in the NF condition. Three different samples were filmed at 333.2 ms frame^{-1} (3 frames s^{-1}) and the obtained movies are played at 3 frames s^{-1}. Foot stomp events at the L- and T-heads are marked with light-blue and red triangles, respectively. (a) Scan area, 90 × 90 nm^2 with 80 × 80 pixels. This movie corresponds to the AFM images shown in Fig. 2c and to the first time course shown in Supplementary Fig. 3c. (b) Scan area, 80 × 80 nm^2 with 100 × 100 pixels. This movie corresponds to the second time course shown in Supplementary Fig. 3c. (c) Scan area, 100 × 100 nm^2 with 80 × 80 pixels.

Supplementary Movie 6 | High-speed AFM movie showing transition between the straight and sharp bend conformations of the L-head. Actin-bound M5-HMM was imaged in the presence of 0.1 μM ADP at 3 frames s^{-1} and the obtained movie is played at 12 frames s^{-1}. Scan area, 90 × 90 nm^2 with 80 × 80 pixels. The images are affected by the double-tip effect.

Supplementary References

1. De La Cruz, E. M. *et al*. The kinetic mechanism of myosin V. *Proc. Natl. Acad. Sci. USA* **96**, 13726-13731 (1999).
2. Sakamoto, T. *et al*. Direct observation of the mechanochemical coupling in myosin Va during processive movement. *Nature* **455**, 128-132 (2008).
3. Forkey, J. N. *et al.* Three-dimensional structural dynamics of myosin V by single-molecule fluorescence polarization. *Nature* **422**, 399-404 (2003).
4. Baker, J. E. *et al.* Myosin V processivity: multiple kinetic pathways for head-to-head coordination. *Proc. Nat.l Acad. Sci. USA* **101**, 5542-5546 (2004).
5. Ando, T. *et al.* A high-speed atomic force microscope for studying biological macromolecules. *Proc. Natl Acad. Sci. USA* **98**, 12468-12472 (2001).
6. Ando, T., Uchihashi, T. & Fukuma, T. High-speed atomic force microscopy for nano-visualization of dynamic biomolecular processes. *Prog. Surf. Sci.* **83**, 337-437 (2008).
7. Burgess, S. *et al.* The prepower stroke conformation of myosin V. *J. Cell Biol.* **159**, 983-991 (2002).
8. Volkmann, N. *et al.* The structural basis of myosin V processive movement as revealed by electron cryomicroscopy. *Mol. Cell* **19**, 595-605 (2005).